AIAA JOURNAL
Vol. 43, No. 12, December 2005

Numerical Study of a Separated–Reattached Flow on a Blunt Plate

Ibrahim E. Abdalla* and Zhiyin Yang†
Loughborough University, Loughborough, England LE11 3TU, United Kingdom

Large-eddy simulation (LES) of transitional separating–reattaching flow on a flat plate with a blunt leading edge has been performed. The Reynolds number based on the uniform inlet velocity and the plate thickness is 6.5×10^3. A dynamic subgrid-scale model is employed in the transitional flow case. The LES results compare reasonably well with the available experimental data. The entire transition process has been visualized by using the LES data, and large-scale vortical structures have been observed at different stages of transition. It is known that different vortex shedding frequencies exist, especially the so-called low-frequency flapping when there is a separation bubble. It is not clear whether all transitional and turbulent separating–reattaching flows have different vortex shedding frequencies. It is also not clear what the working mechanisms are behind the so-called low-frequency flapping as reported widely. These issues are addressed.

Nomenclature

C	=	Smagorinsky model constant
E_p	=	pressure spectra
E_u	=	streamwise velocity spectra
E_v	=	wall-normal velocity spectra
E_w	=	spanwise velocity spectra
f	=	frequency
i	=	streamwise axis index
j	=	wall-normal axis index
k	=	spanwise axis index
$\bar{U}$	=	mean streamwise velocity
U_0	=	freestream velocity
u_{rms}	=	rms value of the streamwise velocity
v_{rms}	=	rms value of the wall-normal velocity
x	=	streamwise axis
x_R	=	mean reattachment length of the separation bubble
y	=	wall-normal axis
y_c	=	shear layer center; location of inflectional point
y_δ	=	edge of the shear layer
z	=	spanwise axis
Δx^+	=	wall-normal mesh size in wall units
Δy^+	=	streamwise mesh size in wall units
Δz^+	=	spanwise mesh size in wall units
ν	=	molecular viscosity

Introduction

SEPARATING–REATTACHING flows occur in a wide variety of practical engineering applications such as airfoils at an angle of attack, reentry vehicles, diffusers, tubomachines, combustors, sudden area change in pipes or ducts, and atmospheric flows over fences and hills. One of the fundamental features of this type of flows is two basic modes of characteristic frequencies. The higher-frequency mode is associated with the usual large-scale motions in the shear layer, whereas the lower-frequency mode reflects overall separation bubble growth/decay dynamics or shear layer flapping as it is frequently called in the literature. The objective of this paper is to shed more light on this feature of separating–reattaching flows.

In a blunt plate geometry, Kiya and Sasaki[1] (hereafter referred to as KS) measured the cross spectrum $|E_{u'v'}|$ and the phase $\phi_{u'v'}$ at the edge and the center of the shear layer at a Reynolds number of 2.6×10^4 based on the freestream velocity and the plate thickness. The cross spectra attain a maximum at the frequency $fx_R/U_\infty \approx 0.5$, which is near the peak frequency of the measured power spectra of the longitudinal velocity and surface pressure fluctuation in the reattachment section. They assumed that these peaks of the spectra correspond to the shedding of large-scale vortices from the separation bubble, which they estimated to be $0.6–0.8\, fx_R/U_\infty$. They also measured the autocorrelation coefficient of the longitudinal velocity fluctuations $R_{u'u'}$, which reveals a long tail observed up to the location $x/x_R \approx 0.5$. Close to separation, at $x/x_R \approx 0.02$, a high-frequency periodic wave is superimposed on the tail, the nondimensional frequency fx_R/U_∞ being approximately 30. They interpreted the high-frequency component as the frequency at which the rolled-up vortices in the shear layer pass through the position of a fixed hot-wire probe. They also suggested that the tail of the autocorrelation curve is associated with the low-frequency flapping motion of the shear layer near the separation line. They attributed the flapping to a large-scale unsteadiness in the bubble, the origin and nature of which was not clear at that time. By studying the cross correlation of the surface pressure fluctuations at two separated locations, $x/x_R = 0.2$ and 1.0, they concluded that the flapping of the shear layer is closely related to the shrinkage and enlargement of the separation bubble. They emphasized that this large-scale unsteadiness is different from the smaller-scale unsteadiness caused by the regular vortex shedding from the bubble, and the representative frequency of the former is much lower than that of the latter by a factor of 6.

Cherry et al.[2] (hereafter referred to as CHL) measured velocity and surface-pressure fluctuations on a blunt plate held normal to a uniform flowfield at a Reynolds number of 3.2×10^4. The flow was laminar before separation, but transition occurred extremely close to separation. Near separation, the measured power spectra for surface-pressure fluctuations were found to be dominated by low-frequency fluctuations. The low-frequency value was estimated to be about one-fifth of the characteristic shedding frequency. Trying to explain the main source of the phenomenon, CHL[2] ruled out any experimental error, side plate or aspect ratio, or tunnel acoustics to be the reason behind the low-frequency unsteadiness. CHL[2] were suspicious about the effect of transition in the shear layer to be the cause. This is because at a very low Reynolds number (3×10^3) their smoke visualization experiment showed a significant low-frequency variability in the instantaneous transition position. However, because transition at the test Reynolds number occurred extremely close to

Received 20 March 2003; revision received 15 April 2004; accepted for publication 29 April 2004.

*Research Student, Department of Aeronautical and Automotive Engineering; i.e.abdalla@lboro.ac.uk.
†Senior Lecturer, Department of Aeronautical and Automotive Engineering; z.yang@lboro.ac.uk.

separation, and due to the fact that the phenomenon appeared in the backward-facing step separations of both Eaton and Johnston[3] and Cherry et al.,[4] where it was already turbulent flow at separation, transition effect was ruled out too. CHL[2] drew the conclusion that "the low-wave number motion appears to be an integral feature of fully turbulent separation." Farther downstream from separation, the spectra become dominated by a broad band shedding of vorticity from the bubble. From the velocity spectra, the most dominant shedding frequency is approximated to a value of $fx_R/U_\infty = 0.7$.

In the numerical simulation of Tafti and Vanka[5] (hereafter referred to as TV), the autocorrelation of the streamwise velocity near the center of the shear layer captured a low-frequency peak about $0.15U_\infty/x_R$, which they attributed to the low-frequency flapping of the shear layer. Superimposed on the low-frequency motion is a high-frequency motion with $f = 4.2U_\infty/x_R$, which they claimed to be caused by a selective high-frequency shedding from the separated shear layer. This new high-frequency vortex shedding from the separated shear layer is twice the predominant rate of shedding ($2.1U_\infty/x_R$) and selectively occurs with the period of the low-frequency flapping. This selective high-frequency shedding from the shear layer has not been distinctly reported by any previous and recent experimental studies. TV[5] suggested that this phenomenon is more prominent at low Reynolds numbers. The autocorrelation of the streamwise velocity fluctuations reported by KS[1] at the center of the shear layer indeed shows a high-frequency content ($f = 30U_\infty/x_R$), which they attributed to the passing of rolled-up vortices through the measurement location. However, the value of KS[1] (50 times the normal shedding frequency) is much higher when compared with the TV[5] case, which is about seven times as large as the normal shedding frequency.

Cherry et al.,[4] Castro and Haque,[6] and Laura et al.[7] detected both the low- and high-frequency modes of unsteadiness for separated flow behind a normal flat plate with a long central splitter plate. However, Ruderich and Fernholz[8] observed no dominant frequencies in their power spectra for the same flow configuration, which led them to believe that there is no flapping of the reattaching shear layer. In the backward-facing step flow, both frequency modes were detected in velocity measurements of Eaton and Johnston.[3] They argued that the observed low-frequency motion on the backward-facing step flow is likely to be a consequence of an instantaneous imbalance between the entrainment rate from the recirculation zone and its resupply near the reattachment. Lee and Sung[9] also detected the two modes of frequency in their measured spectra of surface pressure close to separation in a backward-facing step flow.

It is worth pointing out that, of all of the experimental and numerical work discussed, almost all deal with turbulent separation in the higher-Reynolds-number range with the exception of CHL,[2] at which transition occurs almost at the separation point. Despite the fact that the TV[5] case is a low-Reynolds-number case, the initial condition for TV[5] was generated by superimposing spanwise perturbations on a two-dimensional solution obtained from a previous simulation. The perturbations were applied to the streamwise velocity just upstream of the separating edge, which led to breakdown of the initially two-dimensional unsteady flowfield into three-dimensional turbulence. This indicates that the flow is turbulent prior to the plate leading edge, which hence likely leads to a turbulent separation. The question that arises is; Will transition help to amplify this low-frequency unsteadiness, or will it act as a filter to absorb and damp it? This is going to be investigated in the present study.

Governing Equations and the Numerical Method

The filtered equation expressing conservation of momentum in a Newtonian incompressible flow is written in an explicitly conservative form:

$$\partial_t(\bar{u}_i) + \partial_j(\overline{u_i u_j}) = -\partial_i \bar{P} + 2\partial_j(\nu \bar{S}_{ij}) \tag{1}$$

the strain $\bar{S}_{ij}$ is

$$\bar{S}_{ij} = \tfrac{1}{2}(\partial_i \bar{u}_j + \partial_j \bar{u}_i) \tag{2}$$

and $\bar{P}$ is the physical pressure divided by density.

The mass conservation law is expressed by the zero divergence of the velocity field:

$$\partial_i \bar{u}_i = 0 \tag{3}$$

The equation for pressure is developed by taking the divergence of Eq. (1):

$$\partial_i \partial_t(\bar{u}_i) + \partial_i \partial_j(\overline{u_i u_j}) = -\partial_i \partial_i \bar{P} + 2\partial_i \partial_j(\nu \bar{S}_{ij}) \tag{4}$$

and by using continuity equation (3) one finally obtains

$$\partial_i \partial_i \bar{P} = \nabla^2 \bar{P} = \partial_i H_i \tag{5}$$

$$H_i = \partial_j(-\overline{u_i u_j} + 2\nu \bar{S}_{ij}) \tag{6}$$

Equation (5) is particularly suitable for the time-accurate computation of the pressure in an incompressible flow simulation using linear differencing. The equation can be Fourier transformed in z (a very rapid computational task) to obtain a set of decoupled equations, which in the Cartesian case is

$$\frac{\partial^2 \tilde{P}}{\partial^2 x} + \frac{\partial^2 \tilde{P}}{\partial^2 y} - k_z^2 \tilde{P} = \tilde{R} \tag{7}$$

This process can be performed even when the z derivatives are replaced by the finite difference formulas, provided that z in the simulation is periodic and has an even mesh. For example, the second-order central scheme on an even uniform mesh:

$$\frac{\partial^2 P}{\partial^2 z} = \frac{P_{n-1} - 2P_n + P_{n+1}}{\Delta z^2} \tag{8}$$

can be discrete Fourier transformed to give

$$\frac{\partial^2 P}{\partial^2 z} = -K_z^2 \tilde{P} \tag{9}$$

where

$$K_z = \frac{2\sin(K_z/2)}{\Delta z} \tag{10}$$

and K_z is the usual discrete Fourier wave number.

The two-dimensional equation (7), one for each value of K_z can be solved very quickly even when the geometry is complex as long as it is homogeneous in one direction.

The subgrid-scale stress term

$$\tau_{ij} = \overline{u_i u_j} - \bar{u}_i \bar{u}_j \tag{11}$$

represents the contribution from the subgrid scales and must be modeled. In the present study, the dynamic model[10,11] has been applied. A base subgrid-scale model such as that of Smagorinsky[12] is needed. One then applies a second, coarser spatial filter, called the "test" filter, to the filtered governing equations.

Applying the base[12] model at both filter scales,

$$\tau_{ij} - \tfrac{1}{3}\delta_{ij}\tau_{kk} = -2C\Delta^2|\bar{S}|\bar{S}_{ij} \tag{12}$$

$$T_{ij} - \tfrac{1}{3}\delta_{ij}T_{kk} = -2C(\hat{\Delta}^2)|\hat{\bar{S}}|\hat{\bar{S}}_{ij} \tag{13}$$

Using the Germano identity (see Ref. 10) and following Lilly,[11] C can be evaluated as

$$C = -\frac{1}{2}\frac{L_{ij}M_{ij}}{M_{ij}M_{ij}} \tag{14}$$

This evaluation of C differs from that of Germano et al.[10] expressed as

$$C = -\frac{1}{2}\frac{L_{ij}\bar{S}_{ij}}{M_{ij}\bar{S}_{ij}} \tag{15}$$

In the current simulation C is defined as

$$C = -\frac{1}{2}\frac{\langle L_{ij}M_{ij}\rangle}{\langle M_{ij}M_{ij}\rangle} \tag{16}$$

where the angle brackets represent an average over the homogeneous z direction. The resulting C is a function of time and the inhomogeneous coordinates x and y. In the present study the test-filtered flow quantities were computed by spatial averaging over nine surrounding grid cells.

The explicit second-order Adams–Bashforth scheme is used for the momentum advancement except for the pressure term. The Poisson equation for pressure is solved by using an efficient hybrid Fourier multigrid method. The spatial discretisation is second-order central differencing, which is widely used in large-eddy simulation (LES) owing to its nondissipative and conservative properties. More details of the mathematical formulation and numerical methods in general coordinates have been reported elsewhere by Yang and Voke.[13]

Details of Numerical Computation

Figure 1 shows the computational domain and mesh used in the study. The size of the computational domain is $25D \times 16D \times 4D$ along the x, y, and z axes, respectively, where $D = 10.0$ mm is the plate thickness. The origin of the x coordinate is located $\frac{1}{2}D$ from the leading edge of the plate, and the inflow boundary is at $x = -4.5D$, whereas the outflow boundary is at $x = 20.5D$. The lateral boundaries are at $8D$ from the surface, corresponding to a blockage ratio of 16. It is clear from Fig. 1 that the origin of the lateral direction is the center of the plate, but it is worth pointing out that for all profiles of the mean values the origin will shift to the surface of the plate.

Two simulations were performed. In the first simulation $256 \times 164 \times 64$ cells along the streamwise, wall-normal, and spanwise directions were used. In terms of wall units based on the friction velocity downstream of reattachment at $x/x_R = 2.5$, the streamwise mesh sizes vary from $\Delta x^+ = 11.98$ to $\Delta x^+ = 59.92$, $\Delta z^+ = 24.96$ and at the wall $\Delta y^+ = 11.98$. The time step used in this simulation is $0.005655(D/U_0)$. The simulation ran for 65,000 time steps to allow the transition and turbulent boundary layer to become established, i.e., the flow reached a statistically stationary state, and the averaged results were gathered over a further 312,000 steps with a sample taken every 10 time steps (31,200 samples) and averaged over the spanwise direction too, corresponding to around 63 flow-through or residence times.

In the second simulation the domain dimensions and the mesh cells along the streamwise and spanwise directions are the same as in the first simulation. Along the wall-normal direction the mesh was refined by using 212 cells. In terms of wall units based on the friction velocity downstream of reattachment at $x/x_R = 2.5$, the streamwise mesh sizes vary from $\Delta x^+ = 9.7$ to 48.5, $\Delta z^+ = 20.2$ and at the wall $\Delta y^+ = 2.1$. The time step used in the simulation is $0.001885(D/U_0)$. The simulation ran for 70,000 time steps to allow the transition and turbulent boundary layer to become established, and the averaged results presented later were then gathered over a further 399,000 steps with a sample taken every 10 time steps (39,900 samples) and averaged over the spanwise direction too, corresponding to around 28 flow-through or residence times. Instantaneous flowfields and time traces of velocity components at certain points were also stored during the two simulations for the purpose of visualization and analysis. Comparisons between the two sets of results in terms of flow structures and spectra show little difference, but the second set has better statistical agreement with the available experimental data. All of the results presented in this paper are taken from the second simulation, apart from the spectral analysis part, which is taken from the first simulation as the corresponding running time is longer than the second simulation.

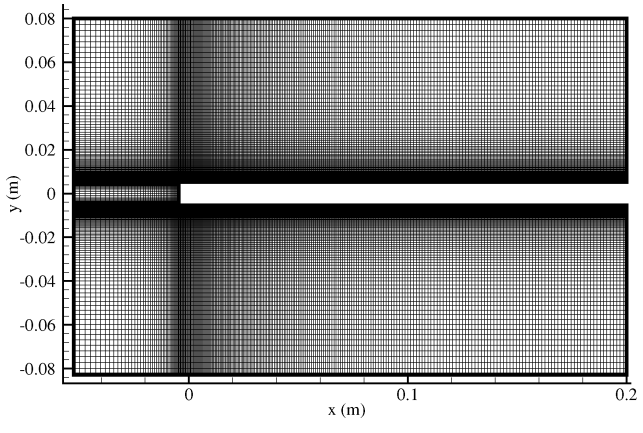

Fig. 1 Computational domain and mesh.

A free-slip but impermeable boundary condition is applied on the lateral boundaries. In the spanwise direction, the flow is assumed to be statistically homogeneous and periodic boundary conditions are used. No-slip boundary conditions are used at all walls. The inflow velocity U_0 is 9.425 m/s, uniform and aligned with the plate. The Reynolds number based on the inflow velocity and plate thickness is 6.5×10^3. At the outflow boundary, a convective boundary condition is applied. Nonuniform grid distributions are used in the x and y directions, with finer resolution in the vicinity of the flat plate to resolve the shear layers. A uniform grid distribution is used in the spanwise direction.

In the present study, the center of the shear layer (y_c) is defined as the y location where the rms value of the streamwise velocity (u_{rms}) attains a maximum value, consistent with the definition of KS.[1] The edge of the shear layer, y_δ, is defined as the locus of points where u_{rms}/U_0 has a value of 2.5%. This definition is consistent with the experimental studies of Djilali and Gartshore[14] and CHL.[2]

Results and Discussion

Mean Flow Variables

The current LES results will be compared with the experimental data by Castro and Epik[15] (hereafter referred to as CE) with the same geometry and Reynolds number. The difference is that CE[15] used a flap to control the length of the bubble in the two cases (with and without freestream turbulence). Also, the blockage ratio of the experiment is approximately four times that of the simulation. Comparisons are done here for the zero-freestream-turbulence case.

Because of the very limited data from CE,[15] the LES results are also compared with KS[1] data and the numerical results by TV.[5] To facilitate comparison, the profiles are plotted as a function of y/x_R at corresponding values of x/x_R, y is measured from the plate surface, and x_R is the mean reattachment length. The measured bubble length is $7.7D$ by Castro and Epik,[15] which is bigger than the simulated bubble length (about $6.5D$). This is a reasonably good agreement taking into account the effect of flap and blockage ratio as mentioned earlier. CHL[2] reported a value of $4.9D \pm 0.05D$ at higher Reynolds numbers ($3.2 \times 10^4 \pm 0.2 \times 10^4$). They also reported that the bubble length started to increase when the Reynolds number was reduced below 3.0×10^4. They attributed this to the gradual extension of the laminar shear layer seen in the visualization of Hillier and Cherry.[16] KS[1] reported a slightly higher value of the mean reattachment length ($5.05D$) for a Reynolds number of 2.6×10^4, whereas TV[5] predicted a value of $6.3D$ for a low-Reynolds-number (1×10^3) case.

Figure 2 compares the mean streamwise velocity distribution $\bar{U}/U_0$ with the experimental data by KS[1] and the numerical results of TV[5] at three streamwise locations. The results show a reasonably good agreement with the data of KS.[1] The predicted peak and the freestream values of the velocity are bigger than those measured by KS.[1] This discrepancy could be mainly due to the blockage effects. The results of TV[5] have a better agreement with the current LES results. The possible explanation is that the Reynolds numbers are relatively low in both simulations and the blockage ratio is the same.

Profiles of the rms values of streamwise velocity, u_{rms}, normalized by U_0, at the same three stations discussed earlier are shown in Fig. 3. The agreement between the LES results and the data of KS[1] and results of TV[5] is good when facts such as the Reynolds

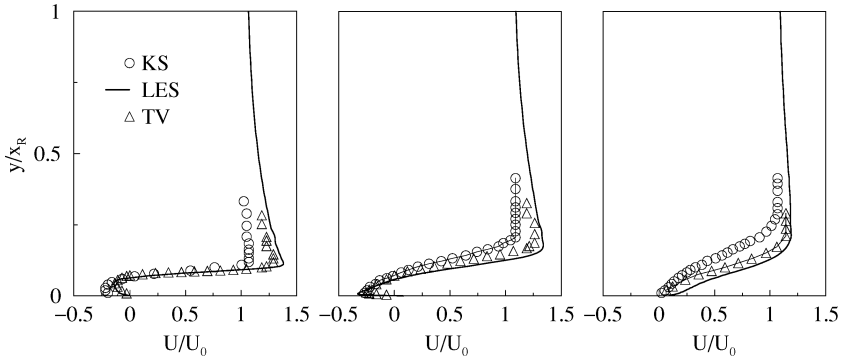

Fig. 2 Profiles of mean streamwise velocity $\bar{U}/U_0$ at three streamwise locations. Also shown are measurements by KS[1] at $Re = 26 \times 10^3$ and numerical results by TV[5] at $Re = 1 \times 10^3$.

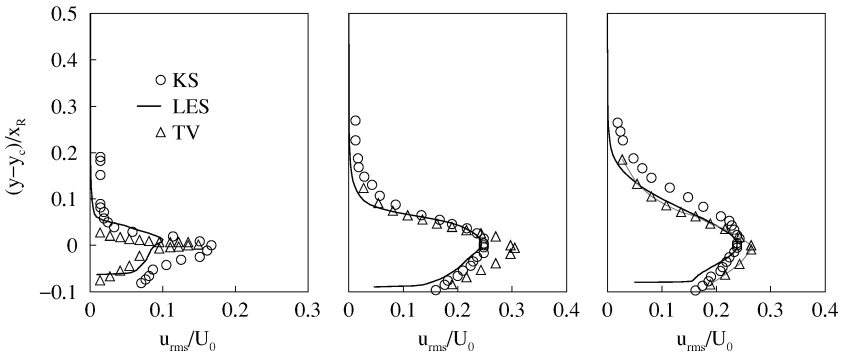

Fig. 3 Profiles of mean streamwise turbulent intensity $u_{\rm rms}/U_0$ at three streamwise locations. Also shown are measurements by KS[1] at $Re = 26 \times 10^3$ and numerical results by TV[5] at $Re = 1 \times 10^3$.

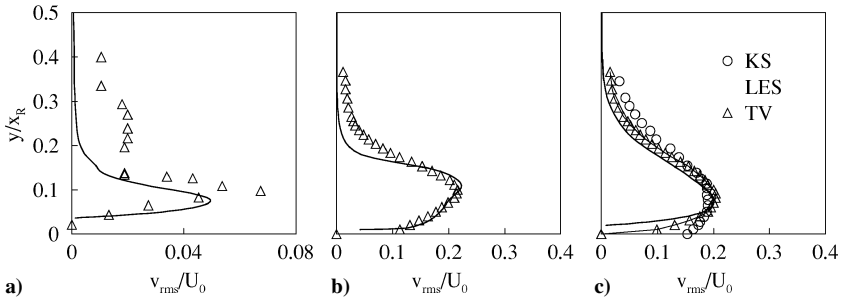

Fig. 4 Profiles of mean streamwise turbulent intensity $u_{\rm rms}/U_0$ at three streamwise locations. Also shown are measurement of KS[1] at $Re = 26 \times 10^3$ and numerical results by TV[5] at $Re = 1 \times 10^3$.

number effects and the differences in blockage ratio are taken into consideration. At the first location ($x/x_R = 0.2$), where the currently predicted flow is still laminar, the peak values of $u_{\rm rms}/U_0$ are smaller than those measured by KS[1] and predicted by TV.[5] The current LES predicts a maximum value of $u_{\rm rms}$ of $0.285U_0$ at $x/x_R = 0.8$ (not shown here). Simulation by TV[5] shows a maximum value of order $u_{\rm rms}/U_0 = 0.32$ in the region $x/x_R = 0.55$–0.7, whereas the measured maximum $u_{\rm rms}$ by KS[1] is $0.26U_0$ at $x/x_R = 0.8$. Other experimental studies[14] have shown maximum $u_{\rm rms}$ of up to $0.3U_0$. Overall, the profiles of $u_{\rm rms}$ show a reasonably good agreement with the data. Figure 4 shows the profiles of $v_{\rm rms}/U_0$ at the same three locations. For $v_{\rm rms}$, measurements have been reported by KS[1] only at $x/x_R = 1.0$. The current LES results show good agreement with the simulation results of TV[5] and KS[1] data as well. In the laminar region at $x/x_R = 0.2$ (Fig. 4a), the peak value predicted by the LES is slightly lower than that predicted by TV.[5] As discussed before, this is likely due to the turbulent separation in the latter; although the Reynolds number is low in TV's[5] simulation, the way they introduced the perturbations would likely lead to turbulent separation.

From this discussion it is clear that the discrepancy between LES results and the data of KS[1] and simulation results of TV[5] appear mainly in the laminar region of the bubble. Good agreement is obtained in other regions where the flow is transitional or turbulent.

The comparison of the Reynolds stresses at reattachment ($x/x_R = 1.0$) with the data of KS[1] and CE[15] is shown in Fig. 5. It can be seen that the LES results overpredict the maximum value for $u_{\rm rms}/U_0$ and $v_{\rm rms}/U_0$ when compared with CE[15] data at the same Reynolds number. Data by CE[15] yield a maximum value for $u_{\rm rms}/U_0$, $v_{\rm rms}/U_0$, and uv/U_0^2 of order 0.19, 0.13, and 0.014. The corresponding predicted values by the LES are 0.25, 0.20, and 0.015, respectively, whereas the data of KS[1] suggest the corresponding values to be of order 0.25, 0.20, and 0.021. It is evident that the LES results are in good agreement with the KS[1] data apart from the $-uv/U_0^2$ variable. The current LES results have a better agreement with the data of CE[15] as far as $-uv/U_0^2$ is concerned. CE[15] compared their data with KS[1] and attributed the difference to be a Reynolds number effect. Measurements by CE[15] at $x/x_R = 1.0$ were obtained with $Re = 3.68 \times 10^3$ because of the upper velocity

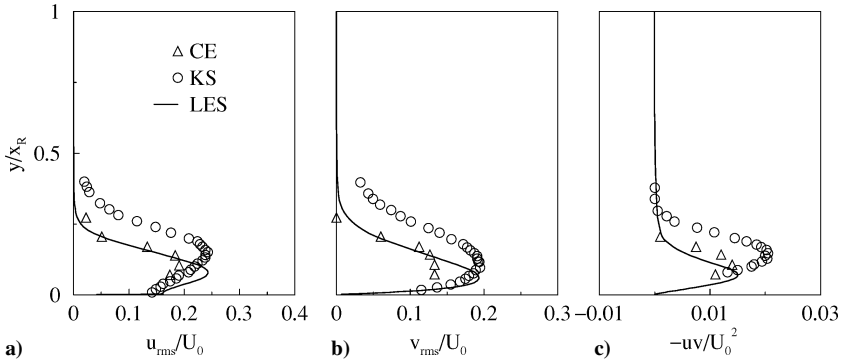

Fig. 5 Reynolds stresses at the mean reattachment location. Also shown are the measurement by KS[1] at $Re = 26 \times 10^3$ and the data of CE[15] at the same location and same Reynolds number.

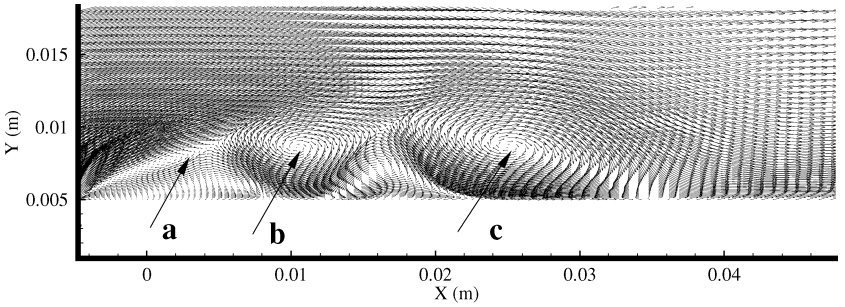

Fig. 6 Laminar bubble before transition.

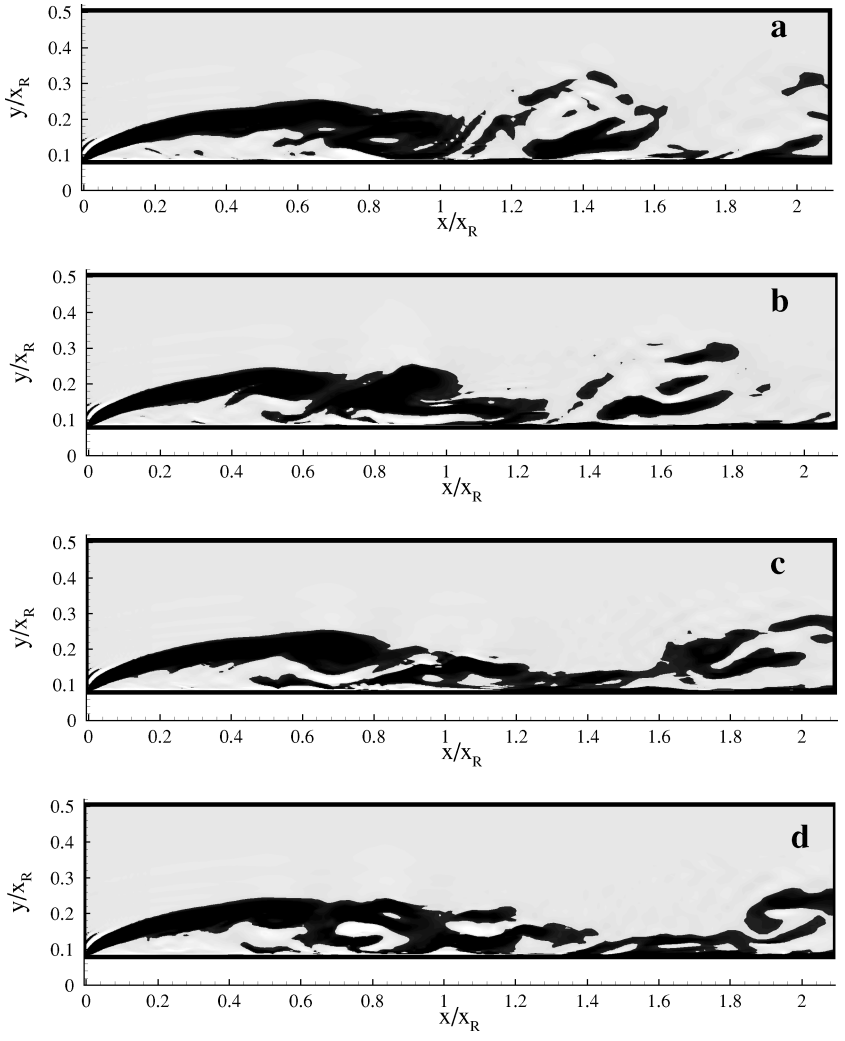

Fig. 7 Instantaneous spanwise vorticity in the (x, y) plane.

limit ≈6 m/s on the miniature pulsed-wire probe. Hancock[17] has shown that in the flat-plate-plus-splitter-plate case, an increase in Re from 3.6×10^3 to 14×10^3 leads to an increase of about 28% in the maximum axial stress at reattachment (attributed to the fact that transition in the separated shear layer occurs earlier). Hillier and Cherry[16] found that the bubble shrank as the Reynolds number increased from 27×10^3 to 34×10^3 (and was then unchanged for higher Reynolds numbers). These two facts clearly indicate that increasing Reynolds numbers will lead to higher values of stress level at reattachment. On the basis of these arguments, CE[15] concluded that at the tested $Re = 6.5 \times 10^3$, it is possible that the stresses at reattachment are actually somewhat higher than those presented in Fig. 5 by an estimated value of order 12%. Overall, this will bring the current LES results to a better agreement with the data of CE[15] which have the same Reynolds number.

Transition Process

The boundary layer develops on either side of the plate, as shown in Fig. 1, and becomes fully turbulent well before the two outflow boundaries. Instantaneously, the flow on either side of the plate can be quite different and not symmetric, just as they would be in reality. In the earliest stages of the simulation, a steady separation bubble appears at the separation line (plate leading edge) and takes a two-dimensional form similar to that found for a laminar separation bubble at low Reynolds number. Later, there could be several bubbles formed just before transition starts. Figure 6 shows the instantaneous flowfield on the (x, y) plane at $z/x_R = 0.2$ at an intermediate stage before transition starts. The bubble has grown in size and extends longitudinally with secondary weak vortices emerging from near the separation line, hanging to the boundary-layer edge (structure a). Such secondary vortices travel downstream and merge with other vortical structures to form a stronger vortical structure c, which is on the way to be shed. In the meantime, the vortical structure b is under development to replace c. Structure b will become stronger by merging with structure a, which is supposed to catch up with it at some distance downstream. Up to this stage, this system of vortical structures behaves in a laminar fashion and can maintain its coherency along the spanwise direction. However, the picture will change drastically when transition initiates.

At a certain stage the free shear layer formed in the bubble becomes inviscidly unstable owing to small disturbances imposed in the simulation, breaking the the strong vortical structures that formed toward the end of the bubble into two smaller vortical structures as the first sign of two-dimensional instability and vortex shedding. The shear layer becomes more unstable, and the newly formed structures break up again, with coherent three-dimensional structures appearing. After several tens of thousands of time steps the flow reaches a statistically stationary state. The transition process can be clearly seen in Fig. 7, which shows the instantaneous spanwise vorticity at various times (1000-time-step interval) in the (x, y) plane at $z/x_R = 0.2$. The vorticity at different z planes looks very similar. In the first half of the bubble, a free shear layer develops and two-dimensional spanwise vortices form. The free shear layer is inviscidly unstable via the Kelvin–Helmholtz mechanism, and any small disturbances present grow downstream with an amplification rate larger than that in the case of viscous instabilities. Farther downstream, the initial spanwise vortices are distorted severely and roll up, leading to streamwise vorticity formation associated with significant three-dimensional motions, eventually breaking down into relatively smaller turbulent structures after the reattachment point and developing into a turbulent boundary layer rapidly afterward.

Velocities and Pressure Spectra

Velocity and pressure correlations are calculated at seven streamwise locations, including a point just before separation ($x/x_R = -0.05$). The other six points are distributed within the separation bubble at $x/x_R = 0.05$, 0.5, and 0.75; at the reattachment $x/x_R = 1.0$; and in the developing boundary layer after reattachment at $x/x_R = 1.25$ and 3.0 and also at three locations along the spanwise dimension $z/x_R = 0.2$, 0.4, and 0.6. For each streamwise location, time traces of velocities U, V, and W and pressure P were stored at four wall-normal locations at $y/x_R = 0.01$, 0.05, 0.13, and 0.2. These four wall-normal positions were designed to include the very near wall region, the center, and the edge of the shear layer. There are 84 points covering the whole domain. A total of 14,000 samples at each point (taken every 20 time steps, with time step $= 6 \times 10^{-6}$ s) were collected, corresponding to 1.68 s. A well-tested code utilizing the Fourier transform methods for autocorrelation was used to process the data. The maximum frequency that can be resolved is 4.166 Kh. All of the figures that follow correspond to data at the z location $z/x_R = 0.2$. Figure 8 shows the exact location of the points discussed in this section, excluding the last two points near the end of the computational domain ($x/x_R = 3.0$).

Close to the separation line and very close to the surface (Fig. 8, point 1) ($x/x_R = 0.05$, $y/x_R = 0.01$), the spectra for the velocity components U, V, and W are shown in Figs. 9a, 9b, and 9c, respectively. At this station very close to the separation line, the spectra do not show any spectacular high- or low-frequency content. The spectra show no trace of the low-frequency peak identified by most of the experiments discussed previously. At the same x location and for $y/x_R = 0.05$ (Fig. 8, point 2), $y/x_R = 0.13$ (Fig. 8, point 3),

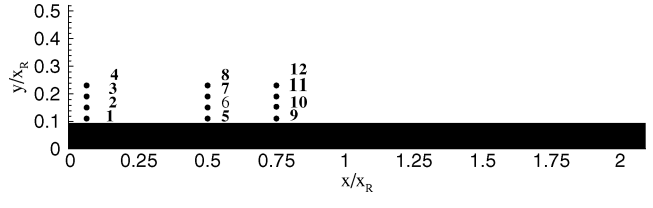

Fig. 8 Locations of points for spectral analysis.

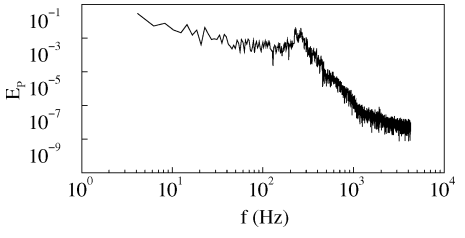

Fig. 10 Spectra for pressure at $x/x_R = 0.5$, $y/x_R = 0.01$.

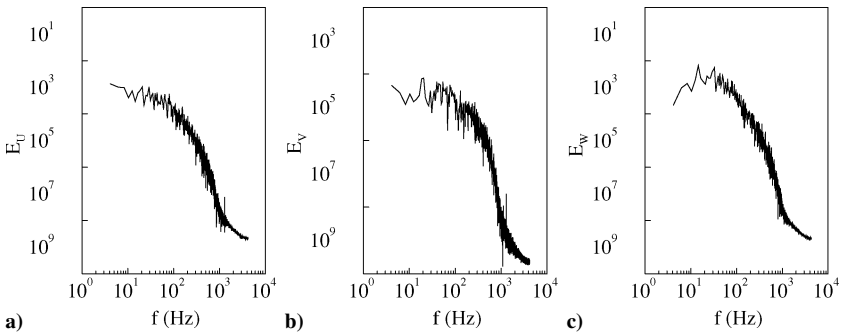

Fig. 9 Spectra for velocity components U, V, and W at $x/x_R = 0.05$, $y/x_R = 0.01$.

and $y/x_R = 0.2$ (Fig. 8, point 4), the pressure and velocity spectra are similar to those in Fig. 9, with no distinguished high- or low-frequency contents appearing. The experimental work of both KS[1] and Cherry et al.[2] emphasized the fact that close to separation, the spectra are dominated by a low-frequency content that they attributed to flapping of the shear layer as discussed previously. However, at this location (the closest to the separation line) the current LES results do not indicate the existence of such a low-frequency peak.

Figure 10 presents the spectra for pressure very close to the surface ($y/x_R = 0.01$) at $x/x_R = 0.5$ (Fig. 8, point 5). The spectra clearly show a peak at the high-frequency band, approximately 126–158 Hz. This is equivalent to 0.7–0.875 U_0/x_R, which is in close agreement with the experimental value of KS,[1] 0.6–0.8 U_0/x_R, and the value, 0.7 U_0/x_R, obtained by CHL.[2] Other studies for separated-reattached flows (different geometries) reported a similar range of this value. For the backward-facing step, Lee and Sung[9] identified this value as $fx_R/U_0 = 0.5$, Mabey[18] as $0.5 \le fx_R/U_0 \le 0.8$, and Driver et al.[19] as $fx_R/U_0 = 0.6$. In the splitter plate with a fence geometry, Laura and Ahmed[7] reported the higher-frequency range as $fx_R/U_\infty = 0.6$–0.9. Spazzini et al.[20] found their maximum to be $fx_R/U_\infty = 1.0$, along with Heenan and Morrison.[21] This higher-frequency peak has been attributed to the shedding of large-scale vortices from the separation bubble.

Moving upward at the same x location $x/x_R = 0.5$, to the position $y/x_R = 0.05$, slightly below the center of the shear layer (Fig. 8, point 6), the spectra of the streamwise, wall-normal velocity and pressure (not shown here) show the regular high shedding frequency 0.7–0.875 U_0/x_R. Moving farther along the y axis to the location $y/x_R = 0.13$ (Fig. 8, point 7), Fig. 11 shows the spectra for the three velocity components, U(a), V(b), W(c), and pressure P(d). This position is approximately at the edge of the shear layer. The spectra for the velocity components reveal shedding at higher frequency, 1000–1125 Hz or 5–6.5 U_0/x_R in addition to the regular high-frequency discussed earlier. This is approximately seven times higher than the regular shedding value. Such higher-frequency shedding from the shear layer has not been reported by any previous experimental studies but by the numerical study of TV.[5] The value estimated by TV[5] is 4.2 U_∞/x_R, which is exactly seven times the regular shedding frequency of 0.6 U_∞/x_R. TV[5] suggested that this phenomenon is more prominent at low Reynolds numbers and may exist also at higher Reynolds numbers but has not been detected due to measurement difficulties. However, it should be noted that the autocorrelation of streamwise velocity fluctuations reported by KS[1] at $x/x_R = 0.02$ at the center of the shear layer indeed shows a very high frequency ($f = 30U_\infty/x_R$), which they have attributed to the passing of rolled-up vortices through the measurement location. Lee and Sung[9] have noticed a similar phenomenon in their experiment behind a backward-facing step, but they attributed the peaks to the tunnel noise from the fan. It is a phenomenon that needs more and careful experimental study to clarify.

Moving downstream to the location $x/x_R = 0.75$ and then moving upward across the same stations as discussed earlier, the same scenario is repeated. Figure 12 shows the spectra for pressure at $y/x_R = 0.01$ (Fig. 8, point 9) very close to the surface. The pressure spectra show only the regular shedding frequency identified in the previously discussed spectra. The spectra at $y/x_R = 0.05$ (Fig. 8, point 10) for the velocity components U, V, and W and pressure P (not shown here) also show only the regular shedding frequency. In Fig. 13 ($y/x_R = 0.13$) (Fig. 8, point 11), panels a, b, c, and d are, respectively, the spectra for the velocity components U, V, and W and pressure P. When compared, respectively, with Figs. 11a–11d (Fig. 8, point 7), which is at the same y location but at $x/x_R = 0.5$, it is noticeable that the higher-frequency shedding is not so strong at this location. At positions farther downstream, $x/x_R = 1.0$ and 1.25 (not shown here), this phenomenon is not as apparent as in previous stations.

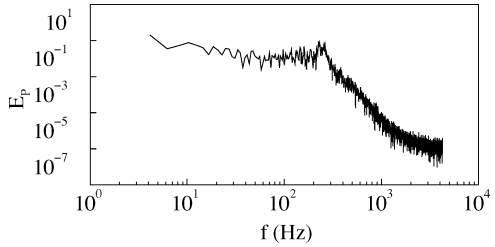

Fig. 12 Spectra for pressure at $x/x_R = 0.75$, $y/x_R = 0.01$ at the surface.

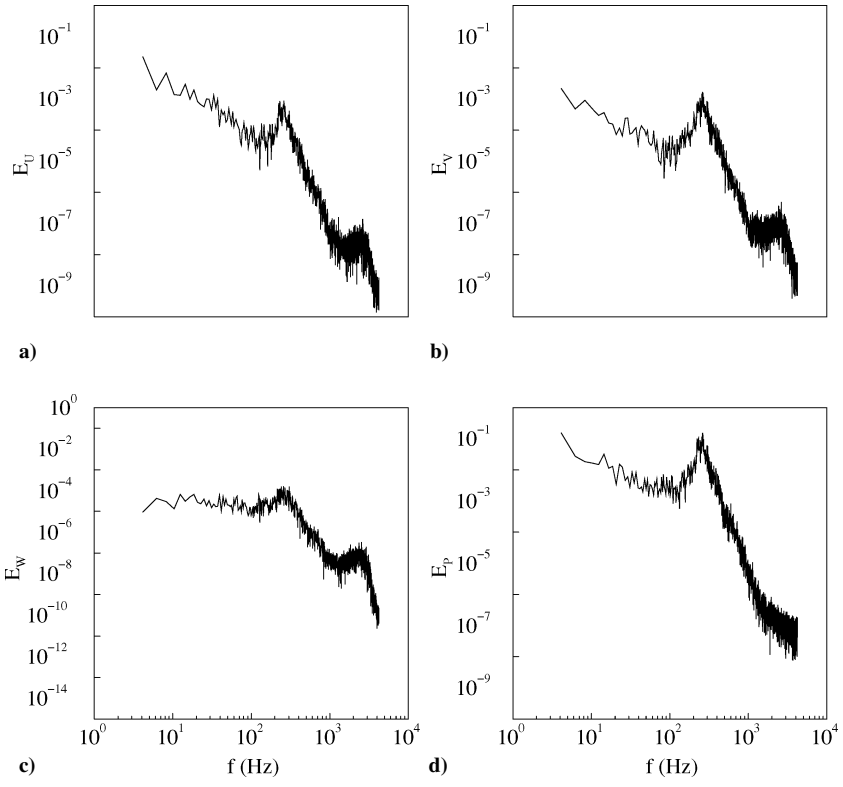

Fig. 11 Spectra for velocity components U, V, W and pressure at $x/x_R = 0.5$, $y/x_R = 0.13$.

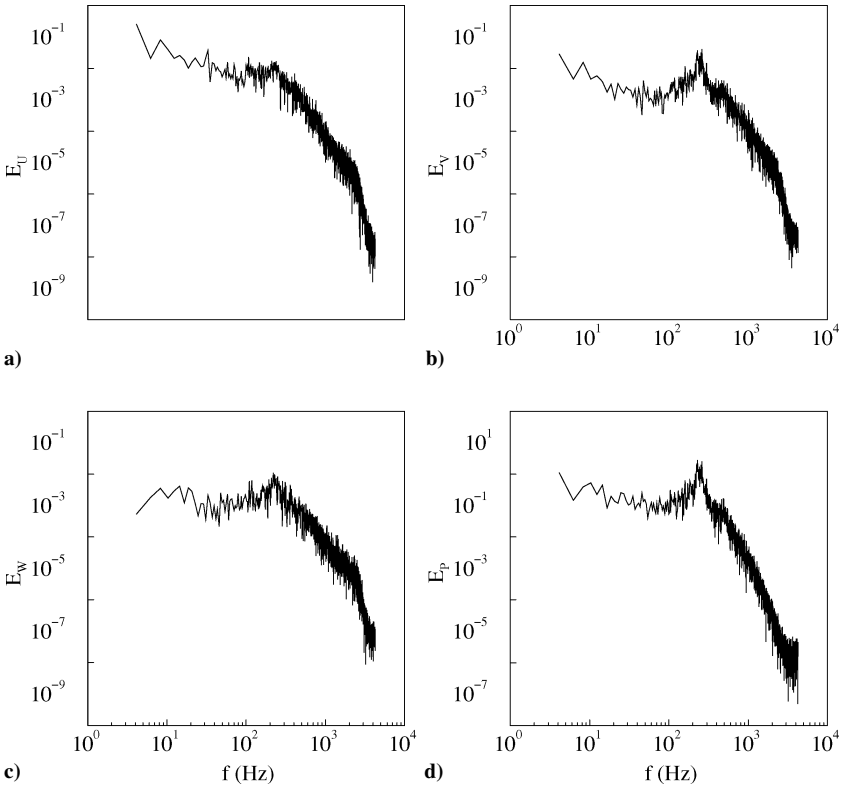

Fig. 13 Spectra for velocity components U, V, and W and pressure at $x/x_R = 0.75$, $y/x_R = 0.13$.

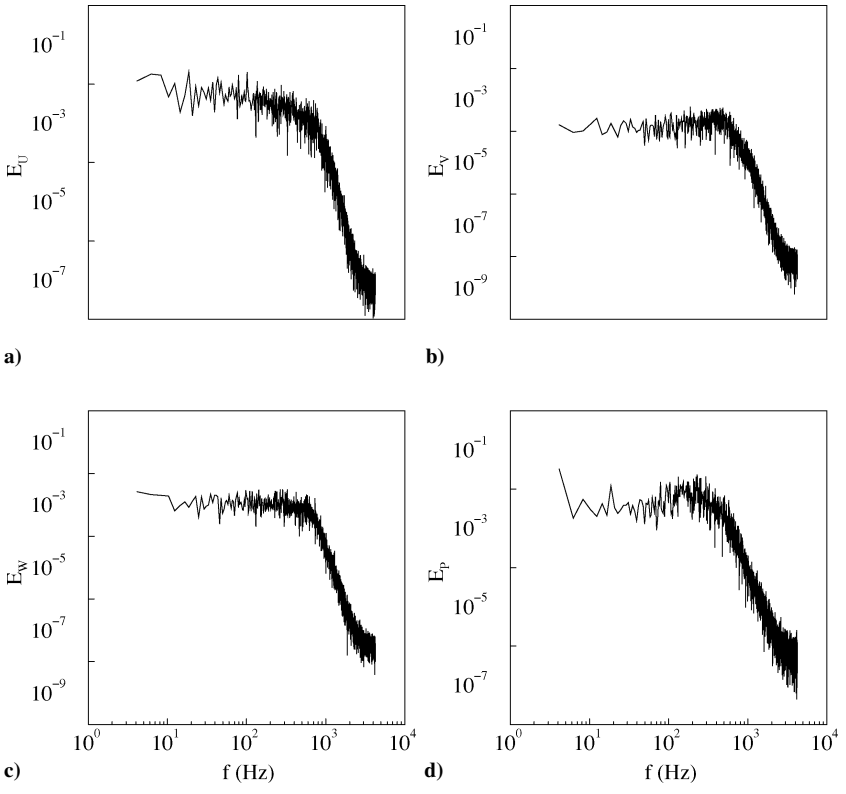

Fig. 14 Spectra for velocity components U, V, and W, and pressure at $x/x_R = 3.0$, $y/x_R = 0.01$.

At the last station ($x/x_R \approx 3.0$) Figs. 14a, 14b, 14c, and 14d present the spectra for the three velocity components U, V, and W and pressure P close to the surface ($y/x_R = 0.01$). At this streamwise location, it is clear that the boundary layer is developing toward a canonical form with no distinguished high- or low-frequency contents. At the same x location and at $y/x_R = 0.05$, 0.13, and 0.2, no distinguished high- or low-frequency contents can be identified in any of the velocity components or pressure spectra (not shown here). Instead the spectra look quite similar to that of a fully developed turbulent boundary layer. In addition, from the spectra at all the points shown there is no indication of the so-called low-frequency flapping.

Large-Scale Structures

Shown in Figs. 15a–15d are low-pressure isosurfaces, $P = -0.1\ \rho_0 U_0^2$, at four different times. It can be seen from Fig. 15a that two-dimensional vortical structures (Kelvin–Helmholtz's

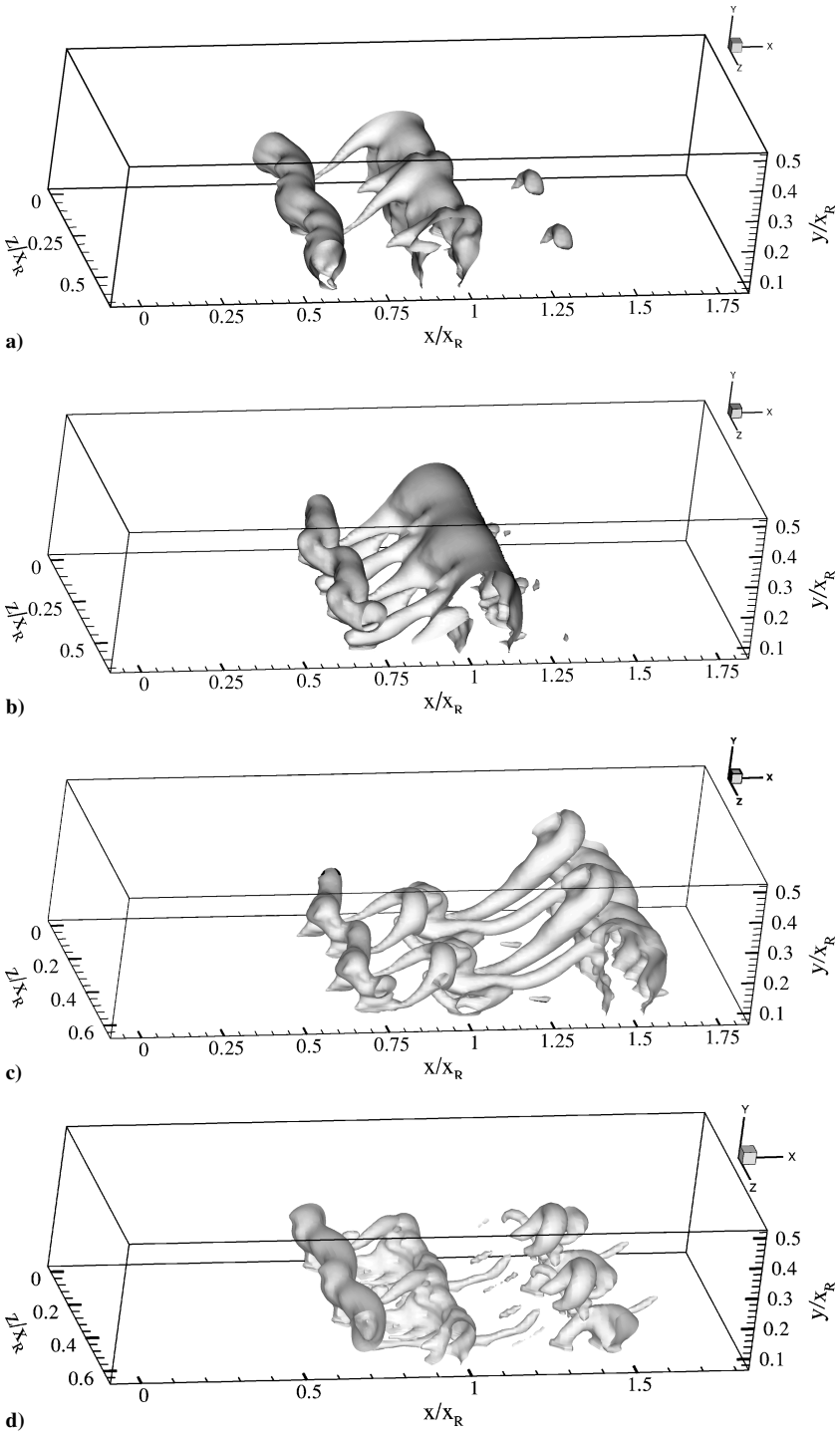

Fig. 15 Low pressure isosurfaces showing the break-up of the k-h rolls into smaller scale structures downstream of reattachment at a) $t = 295.95\ D/U_0$, b) $t = 326.1\ D/U_0$, c) $t = 395.9\ D/U_0$, and d) $t = 427.9\ D/U_0$.

billows) exist at the early stage of the bubble, oscillate in the spanwise direction, and grow in size and become more distorted as they travel downstream. The initially shed spanwise roll becomes severely distorted owing to three-dimensional motion setting in. At this stage, it can clearly be seen that Λ-shaped vortical structures start to form. However, the large-scale coherency of the flow is still observed, with the original Kelvin–Helmholtz billows being stretched into big Λ-shaped vortices. These vortices impinge on the wall and then stretch into big archlike vortices as they are convected downstream (Fig. 15c). However, Λ-shaped vortices persist a considerable distance downstream after reattachment, as can be seen from Fig. 15d. In their numerical simulation of the unsteady separated flow over a blunt plate, TV[5] concluded that the separation bubble is characterized by large coherent structures in the form of spanwise vortices. The Λ-shaped vortical structures identified in the present study were also identified in the LES results of Yang and Voke[22] and are consistent with the idea put forward by Kiya and Sasaki[23] from their experimental study. The persistence of the Λ-shaped vortices is likely to be the reason behind the slow relaxation of the mean streamwise toward canonical turbulent boundary-layer profiles.

Conclusions

Large-eddy simulation has been performed to study numerically the transitional flow over a blunt plate held normal to a uniform stream. The LES results compare reasonably well with the available

experimental data. The transition process leading to breakdown to turbulence has been elucidated and visualized.

The current LES of low-Reynolds-number transitional separated boundary-layer study does not show the low frequency that most of the experiments have identified and that are believed to be due to the flapping of the shear layer. KS[1] estimated this frequency to be of the order $0.2\ U_0/x_R$. Based on the data of KS,[1] this is equivalent to 50 Hz. In the current LES, the maximum frequency that can be resolved is 4.166 kHz ($50\ U_0/x_R$). The sampling was carried out over 264 x_R/U_0 time unit. If we roughly assume that the low frequency should be of the same order as that of KS,[1] then our samples are able to cover 53 low-frequency cycles. This low frequency, which has been identified in most of the experiments, is not captured in the current LES study. TV[5] carried out sampling over a period of time that was equivalent to three low-frequency cycles, and their data captured the low-frequency phenomenon. However, there is a major difference between our case and almost all of the cases we are referring to. Our case is transitional with a pure two-dimensional laminar region at separation and almost up to $x = 0.25\ x_R$, as discussed previously. We believe that the laminar part of the bubble works as a filter to filter out this low-frequency flapping of the shear layer. The experiment by Cherry et al.[2] deals with transitional separation on the same geometry used in this computations, but transition occurs extremely close to separation. At very low Reynolds numbers, their smoke visulization showed low-frequency variability in the instantaneous transition position but not in the laminar part. However, measurements made in the same model with a high level of grid-generated turbulence in the freestream showed a marked contribution at low frequencies.

Based on this, it may be concluded that "the low-wavenumber motion appears to be an integral feature of a fully turbulent separation." KS[1] proposed that the reason behind the flapping observed most clearly near the separation line is that the cross-sectional dimensions of the rolled-up vortices are at least comparable to the spatial extent of the flapping. All of these arguments indicate that two factors should exist for the low-frequency mode to be detected: 1) there must exist some sort of turbulent vortical structures and 2) the cross-sectional dimensions of the these vortical structures are weak and at least comparable to the spatial extent of the flapping. At reattachment, KS[1] estimated the average center of the vortices to be at about $0.2\ x_R$ from the plate surface and the average longitudinal distance between the vortices to be 0.7–0.8 x_R. However, there is no information available regarding the structure of the rolled-up vortices at which the spatial extent of the flapping can overcome and hence dominate the dynamic of the flow. Usually, at separation, a primary weak vortical structure develops and becomes stronger as it approaches the reattachment region by merging with another vortical structure, as described in many studies. Thus in the vicinity of the separation line it is expected that the the lateral and longitudinal dimensions of the vortices will be quite small despite the fact that they are coherent along the spanwise direction. We believe that this low-frequency mode in separated–reattached flows will be more apparent in the case of turbulent separation where rolled-up vortices appear even at separation line. Therefore it may be drawn from the current study that the low-frequency mode will probably not occur in low-Reynolds-number transitional separated–reattached flows.

Acknowledgments

The computations were carried out on a Cray T3E at Manchester University, funded by the Engineering and Physical Science Research Council under the Large-Eddy Simulation-UK2 consortium. Special thanks to Paul Denman, who provided the code used in processing the data for spectral analysis.

References

[1]Kiya, M., and Sasaki, K., "Structure of a Turbulent Separation Bubble," *Journal of Fluid Mechanics*, Vol. 137, 1983, pp. 83–113.

[2]Cherry, N. J., Hillier, R., and Latour, M. E. M. P., "Unsteady Measurements in a Separating and Reattaching Flow," *Journal of Fluid Mechanics*, Vol. 144, 1984, pp. 13–46.

[3]Eaton, J. K., and Johnston, J. P., "A Review on Subsonic Turbulent Flow Reattachment," *AIAA Journal*, Vol. 19, No. 9, 1981, pp. 1093–1100.

[4]Cherry, N. J., Hillier, R., and Latour, M. E. P., "The Unsteady Structure of Two-Dimensional Separated and Reattaching Flows," *Journal of Wind Engineering and Industrial Aerodynamics*, Vol. 11, Nos. 1–3, 1983, pp. 95–105.

[5]Tafti, D. K., and Vanka, S. P., "A Three-Dimensional Numerical Study of Flow Separation and Reattachment on a Blunt Plate," *Physics of Fluids A*, Vol. 3, No. 12, 1991, pp. 2887–2909.

[6]Castro, I. P., and Haque, A., "The Structure of a Turbulent Shear Layer Bounding a Separation Region," *Journal of Fluid Mechanics*, Vol. 179, 1987, pp. 439–468.

[7]Laura, M. H., Ahmed, M. N., and William, M. H., "Wall-Pressure-Array Measurements Beneath a Separating/Reattaching Flow Region," *Physics of Fluids*, Vol. 15, No. 3, 2003, pp. 706–717.

[8]Ruderich, R., and Fernhholz, H. H., "An Experimental Investigation of a Turbulent Shear Flow with Separation, Reverse Flow and Reattachment," *Journal of Fluid Mechanics*, Vol. 163, 1986, pp. 283–322.

[9]Lee, I., and Sung, H. J., "Characteristics of Wall Pressure Fluctuations in Separated and Reattaching Flow over a Backward-Facing Step," *Experiments in Fluids*, Vol. 30, No. 3, 2001, pp. 262–272.

[10]Germano, M., Piomelli, U., Moin, P., and Cabot, W. H., "A Dynamic Subgrid-Scale Eddy Viscosity Model," *Physics of Fluids A*, Vol. 3, No. 7, 1991, pp. 1760–1765.

[11]Lilly, D. K., "A Proposed Modification of the Germano Subgrid-Scale Closure Method," *Physics of Fluids A*, Vol. 3, No. 3, 1992, pp. 633–635.

[12]Smagorinsky, J., "General Circulation Experiments with the Permitive Equations, Part I: The Basic Experiment," *Monthly Weather Review*, Vol. 91, No. 3, 1963, pp. 99–154.

[13]Yang, Z., and Voke, R. P., "Large-Eddy Simulation of Separated Leading-Edge Flow in General Co-Ordinates," *International Journal for Numerical Methods in Engineering*, Vol. 49, No. 5, 2000, pp. 681–696.

[14]Djilali, N., and Gartshore, I. S., "Turbulent Flow Around a Bluff Rectangular Plate. Part I: Experimental Investigation," *Journal of Fluids Engineering*, Vol. 113, No. 1, 1991, pp. 51–59.

[15]Castro, I. P., and Epik, E., "Boundary Layer Development After a Separated Region," *Journal of Fluid Mechanics*, Vol. 374, 1998, pp. 91–116.

[16]Hillier, R., and Cherry, N. J., "The Effect of Stream Turbulence on Separation Bubble," *Journal of Wind Engineering and Industrial Aerodynamics*, Vol. 8, Nos. 1–2, 1981, pp. 49–58.

[17]Hancock, P. E., "Reynolds Number Effects in Separated Flows," *Advances in Turbulence V*, edited by R. Benzi, Kluwer, Dordrecht, The Netherlands, 1995, pp. 184–189.

[18]Mabey, D. G., "Analysis and Correlation of Data on Pressure Fluctuations in Separated Flow," *Journal of Aircraft*, Vol. 9, No. 9, 1972, pp. 642–645.

[19]Driver, D. M., Seegmiller, H. L., and Marvin, J. G., "Time-Dependent Behaviour of Reattaching Shear Layer," *AIAA Journal*, Vol. 25, No. 7, 1987, pp. 914–919.

[20]Spazzini, P. G., Iuso, G., Onorato, M., Zurlo, N., and Di Cicca, G. M., "Unsteady Behaviour of Back-Facing Step Flow," *Experiments in Fluids*, Vol. 30, No. 5, 2001, pp. 551–561.

[21]Heenan, A. F., and Morrison, J. F., "Passive Control of Pressure Fluctuations Generated by Separated Flow," *AIAA Journal*, Vol. 36, No. 6, 1998, pp. 1014–1022.

[22]Yang, Z., and Voke, R. P., "Large-Eddy Simulation of Boundary Layer Separation and Transition at a Change of Surface Curvature," *Journal of Fluid Mechanics*, Vol. 439, 2001, pp. 305–333.

[23]Kiya, M., and Sasaki, K., "Structure of Large-Scale Vortices and Unsteady Reverse Flow in the Reattaching Zone of a Turbulent Separation Bubble," *Journal of Fluid Mechanics*, Vol. 120, 1985, pp. 219–244.

K. Fujii
Associate Editor